2005

Nuclear Properties of Nearby Spiral Galaxies From Hubble Space Telescope NICMOS Imaging and STIS [Space Telescope Imaging Spectrograph] Spectroscopy

M. A. Hughes
University of Hertfordshire

David Axon
Rochester Institute of Technology

John Atkinson
University of Hertfordshire

A. Alonso-Herrero
Consejo Superior de Investigaciones Científicas

C. Scarlata
ETH Zuerich

See next page for additional authors

Recommended Citation
M. A. Hughes et al 2005 AJ 130 73 https://doi.org/10.1086/430531

Nuclear Properties of Nearby Spiral Galaxies from Hubble Space Telescope NICMOS imaging and STIS Spectroscopy.[1]

M. A. Hughes[1], D. Axon[11], J. Atkinson[1], A. Alonso-Herrero[2], C. Scarlata[7], A. Marconi[4], D. Batcheldor[1], J. Binney[6], A. Capetti[5], C. M. Carollo[7], L. Dressel[3], J. Gerssen[12], D. Macchetto[3], W. Maciejewski[4,10], M. Merrifield[8], M. Ruiz[1], W. Sparks[3], M. Stiavelli[3], Z. Tsvetanov[9],

ABSTRACT

We investigate the central regions of 23 spiral galaxies using archival NICMOS imaging and STIS spectroscopy. The sample is taken from our program to determine the masses of central massive black holes (MBH) in 54 nearby spiral galaxies. Stars are likely to contribute significantly to any dynamical central mass concentration that we find in our MBH program and this paper is part of a series to investigate the nuclear properties of these galaxies. We use the Nuker law to fit surface brightness profiles, derived from the NICMOS images, to look for nuclear star clusters and find possible *extended* sources in 3 of the 23 galaxies studied (13 per cent). The fact that this fraction is lower than that inferred from optical *Hubble Space Telescope* studies is probably due to the greater spatial resolution of those studies. Using R-H and J-H colors and equivalent widths of Hα emission (from the STIS spectra) we investigate the nature of the stellar population with evolutionary models. Under the assumption of hot stars ionizing the gas, as opposed to a weak AGN, we find that there are young stellar populations ($\sim$10–20 Myr) however these data do not allow us to determine what percentage of the

[1]Centre for Astrophysical Research, STRI, University of Hertfordshire, Hatfield, Hertfordshire, AL10 9AB, UK.

[2]Departamento de Astrofisica Molecular e Infrarroja, CSIC, Madrid, Spain.

[3]Space Telescope Science Institute, 3700 San Martin Drive, Baltimore, MD 21218

[4]INAF-Osservatorio Astrofisico di Arcetri, Largo E. Fermi 5, 50125 Firenze, Italy

[5]INAF-Osservatorio Astronomico di Torino, I-10025 Pino Torinese, Italy.

[6]Oxford University, Theoretical Physics, Keble Road, Oxford, OX1 3NP, UK

[7]Eidgenoessische Technische Hochshule Zuerich, Hoenggerberg HPF G4.3, CH-8092 Zuerich, Switzerland

[8]School of Physics and Astronomy, University of Nottingham, NG7 2RD, UK

[9]Center for Astrophysical Sciences, Johns Hopkins University, 239 Bloomberg Center for Physics & Astronomy, 3400 North Charles Street, Baltimore, MD 21218

[10]Obserwatorium Astonomiczne Uniwersytetu Jagiellońskiego, Poland

[11]Deptartment of Physics, RIT, 84 Lomb Memorial Dr., Rochester, NY 14623-5603

[12]Department of Physics, University of Durham, Rochester Building, Science Laboratories, South Road, Durham, DH1 3LE, UK

total nuclear stellar population they form. Also, in an attempt to find any unknown AGN we use [N II] and [S II] line flux ratios (relative to Hα) and find tentative evidence for weak AGN in NGC 1300 and NGC 4536.

Subject headings: galaxies: nuclei—galaxies: spiral

1. Introduction

The most impressive result from studies of Massive Black Holes (MBHs) in recent years has been the discovery that the mass of the central black hole is correlated with other properties of the galaxy, such as bulge mass (e.g. Kormendy & Richstone 1995; Marconi & Hunt 2003) and stellar velocity dispersion (Ferrarese & Merritt 2000; Gebhardt et al. 2000). Consequently, it is prudent for any thorough investigation of MBHs to include a detailed study of the center of the galaxy in question. With this in mind, this paper forms part of a series where we investigate the central regions of galaxies from our Hubble Space Telescope (HST) program to find massive black holes in nearby spiral galaxies (GO:8228, PI: D. Axon). The sample is limited to galaxies within a recessional velocity less than 2000 kms^{-1} that are known to have Hα emission from ground based observations. The good spectra and images, and a description of the sample, are presented in Hughes et al. (2003) (Hereafter H03) and Scarlata et al. (2004) (Hereafter S04). The first black hole mass estimates from the program are presented in Marconi et al. (2003), for NGC 4041 and Atkinson et al. (submitted), for NGC 1300 and NGC 2748.

One aspect of galaxy centers, which may have important consequences for black hole mass measurements is the presence of nuclear star clusters. HST observations have played a major role in showing that many (50%+) spiral galaxies have identifiable cores which are photometrically and morphologically distinct from the surrounding bulge (e.g. Böker et al. 2002; Carollo et al. 2002). Such compact luminous sources are generally believed to be nuclear star clusters and, in some cases, this has been demonstrated with spectroscopy (e.g. Böker et al. 2001; Walcher et al. 2003; Colina et al. 2002). The reason that these clusters may be important for black hole mass estimates is that invariably the region over which the central mass is determined includes the region occupied by the cluster. Thus, if the cluster mass is significant with respect to the black hole mass then it needs to be taken into account.

Although quantifying the mass of the central stellar populations is beyond the scope of this paper, we attempt to determine other useful properties of the central regions of the galaxies. Specifically, this paper is a companion to S04 in which we quantified the profile of the bulges from

[1]Based on observations with the NASA/ESA Hubble Space Telescope obtained at the Space Telescope Science Institute, which is operated by the Association of Universities for Research in Astronomy, Inc., under NASA contract NAS 5-26555.

the STIS images using the NUKER law profile (Lauer et al. 1995) and looked for the presence of nuclear star clusters. The first aim of this paper is to re-use the NUKER profile and apply it to archival NICMOS images of galaxies from our sample. Since near-infrared images are not as affected by dust obscuration as the STIS images these provide the opportunity of producing a clearer view of the central bulge, and a better way of quantifying the shape of the bulge. The second purpose of this paper is to use the spectral information from our STIS program (Hughes et al. 2003) and the color information from both our STIS images and archival NICMOS images in an attempt to quantify the age of the central stellar population.

The structure of this paper is as follows, In §1.1 we describe the selection of the sample of spiral galaxies, the STIS spectroscopic observations and the reduction of the archival NICMOS images. In §2 we produce surface brightness profiles from the NICMOS images to look for central sources. In §3 we investigate the ages of the stellar populations at the centers of galaxies using both color information from the NICMOS and STIS images and STIS spectroscopy.

1.1. The Sample Selection

The complete list of galaxies is presented in table 1 in H03 and in Table 1 (this paper) we list those galaxies for which we were able to obtain archival NICMOS H-band images. All the galaxies are classified as late-type spirals and are nearby, having recessional velocities of less than $2000\,\mathrm{km\ s^{-1}}$.

The original purpose of the STIS images was to locate the exact position of the nucleus of each galaxy so that spectroscopic apertures could be accurately placed. Such 'acquisition images' were taken using the F28X50LP longpass filter. They are optical (central wavelength 7230 Å), and are approximately equivalent to R-band. For each galaxy, 2 acquisition images were taken to acquire the nucleus and 3 longslit apertures were placed to determine the nuclear gas disk kinematics. The pixel size is $0.05''\mathrm{pixel}^{-1}$, and the field of view is $5''\times5''$. Integration times of the images vary from 20 to 60 seconds. The STIS images were reduced by the Flight Software (FSW) involving the subtraction of a single bias number and the removal of hot pixels. See chapter 8 of the STIS Instrument Handbook.

Spectra of the galaxy centers covered 5 emission lines [N II] (6549.9 Å), Hα (6564.6 Å), [N II] (6585.3 Å) and [S II] (6718.3 & 6732.7 Å). These spectra are being used to map the velocity fields of nuclear gas disks so that central mass concentrations can be measured. The spectra are described in more detail in H03. Briefly, for each galaxy three slits were placed, one on the brightest central source (presumed to be the nucleus, unless obscured by dust) with 2 other, parallel slits 0.1 arcsec either side. In this paper, we use these spectra for another purpose; to estimate the age of stellar populations at the centers of the galaxies (see §3).

Table 1. The sample of 23 spiral galaxies with archival NICMOS images

Galaxy Name	Morphological Type	Nuclear Activity	Rec. Vel. (km s^{-1})	Inclination (degrees)
NGC 0157	SAB(rs)bc	...	1589	55
NGC 0289	SAB(rs)bc	...	1451	40
NGC 1300	(R')SB(s)bc	...	1409	49
NGC 2748	SAbc	(H II)	1741	73
NGC 2903	SB(s)d	H II (H II)	626	56
NGC 2964	SAB(r)bc	H II (H II)	1446	58
NGC 3259	SAB(rs)bc	...	1929	63
NGC 3310	SAB(r)bc pec	H II (H II)	1208	31
NGC 3949	SA(s)bc	H II (H II)	1021	56
NGC 4030	SA(s)bc	...	1475	40
NGC 4258	SAB(s)bc	L/S1.9 (S1.9)	674	72
NGC 4303	SAB(rs)bc	H II/S2 (H II)	1619	19
NGC 4389	SB(rs)bc pec	...	940	54
NGC 4527	SAB(s)bc	H II/L (T2)	1776	70
NGC 4536	SAB(rs)bc	H II (H II)	1846	59
NGC 5005	SAB(rs)bc	S2/L (L1.9)	1153	67
NGC 5054	SA(s)bc	...	1704	54
NGC 5055	SA(rs)bc	H II/L (T2)	726	56
NGC 5248	(R) SB(rs)bc	S2/H II (H II)	1248	51
NGC 5879	SA(rs)bc?	L (T2/L2)	1049	74
NGC 6384	SAB(r)bc	L (T2)	1780	60
NGC 6951	SAB(rs)bc	L/S2 (S2)	1705	42
NGC 7331	SA(s)b	L (T2)	992	75

Note. — Morphological classification and activity status taken from NASA Extragalactic Database (NED) with classification shown in parenthesis taken from Ho, Filippenko, & Sargent (1997), where H II=H II nuclei, S=Seyfert nuclei, L=LINER, T=Transition nuclei. 'Rec. Vel.' is the recessional velocity corrected for Virgo-centric infall (LEDA). Inclination is the angle between the polar axis and the line of sight, in degrees (LEDA).

The *HST* archive was used to search for NICMOS observations for the galaxies in our sample. We found NIC2 F160W images (1.60μm, similar to a ground-based H-band filter) for 23 galaxies, and for 6 galaxies we found NIC2 F110W filter images (1.10μm, similar to a ground-based J-band filter). Many of the images were observed as part of an *HST* snapshot programme by members of our team and appear in Carollo et al. (2002). The pixel size of the images is 0.076" pixel^{-1}, which produces a field of view of $19.2'' \times 19.2''$. The images were taken as part of a number of programs, with integration times of between 384 and 640 seconds. The images were reduced using NicRed (McLeod 1997). The data reduction involved subtraction of the first readout, dark current subtraction on a readout-by-readout basis, correction for linearity and cosmic ray rejection (using FULLFIT), and flat fielding. In-orbit darks with sample sequences and exposure times corresponding to those of the observations were obtained from other programs close in time. Generally between 10 to 20 darks were averaged together (after subtraction of the first readout) for a each sample sequence. If more than one exposure for a given galaxy was taken, the images were shifted to a common position using fractional pixel offsets and combined to create the final images. Since the images were well sampled, any loss in resolution through using this technique should not be significant.

2. Surface Brightness Profiles and the Presence of Central Sources

Surface brightness profiles have been used as an important diagnostic for inferring the presence of resolved, central sources in galactic nuclei. Böker et al. (2002) presented SBPs derived from *WFPC2* F814W images and found many well resolved central sources. The presence of a central source is indicated by an inflexion in the profile at small radii, see figure 1. Without spectroscopy, such as performed by Böker et al. (2001) on NGC 4449 (who found a 6-10 Myr stellar population) or Walcher et al. (2003), we cannot be confident of the nature of these central sources. However, the general assumption by most authors is that they are probably star clusters.

Over the past few years, analysis of central sources has been performed for a large number of disk galaxies using *HST* images, in particular using *WF/PC 1* (Phillips, Illingworth, MacKenty, & Franx 1996), *WFPC 2* (Carollo & Stiavelli 1998; Carollo, Stiavelli, & Mack 1998) and NICMOS (Carollo et al. 2002; Seigar et al. 2002). The main inference of these studies has been that central sources are a common feature of galaxy centers.

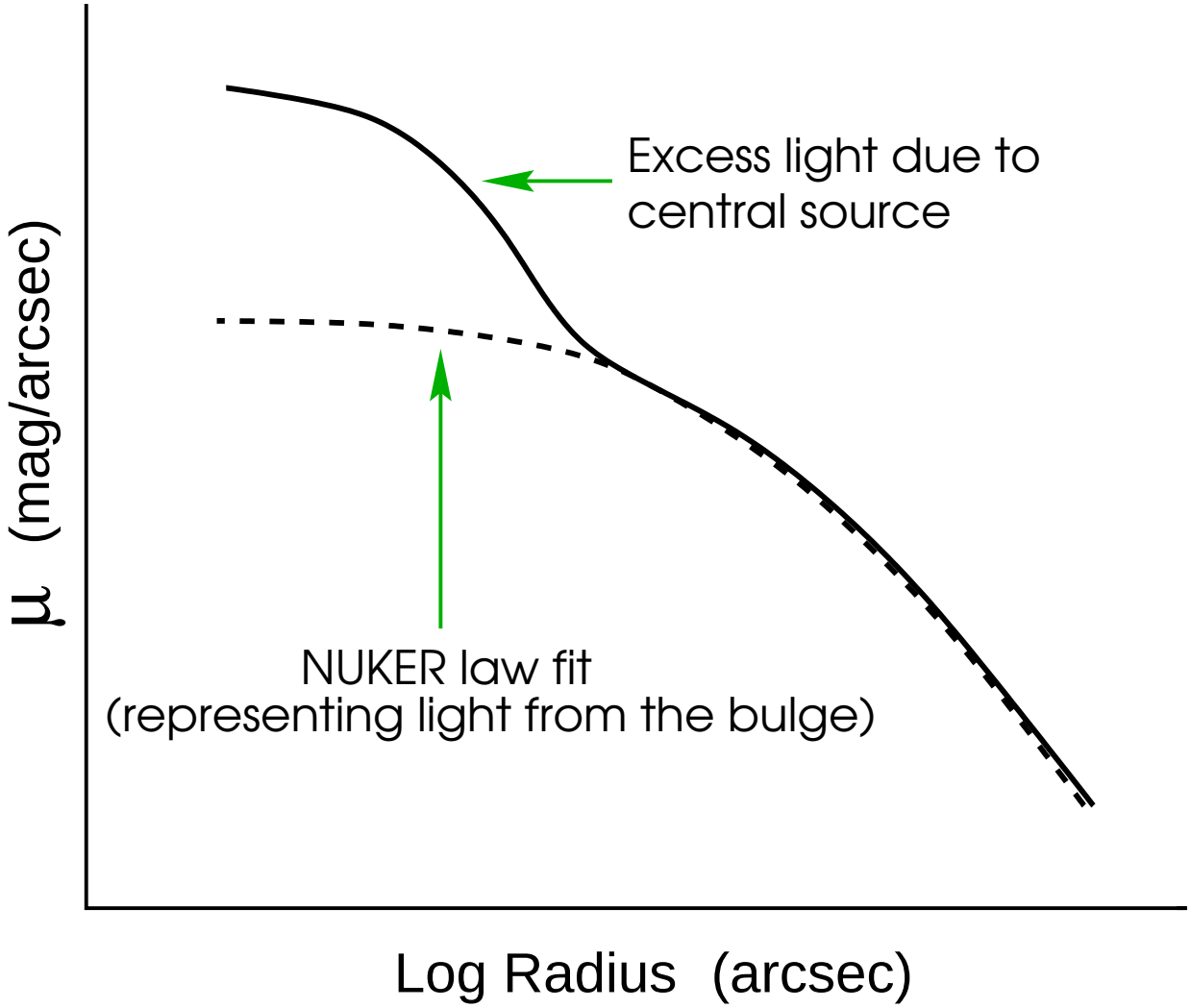

Fig. 1.— An idealised picture of a surface brightness profile (SBP). In several cases, a clear bump is seen that cannot be accounted for in the standard Nuker law model. This excess light is assumed to be from a compact luminous source, possibly a nuclear star cluster.

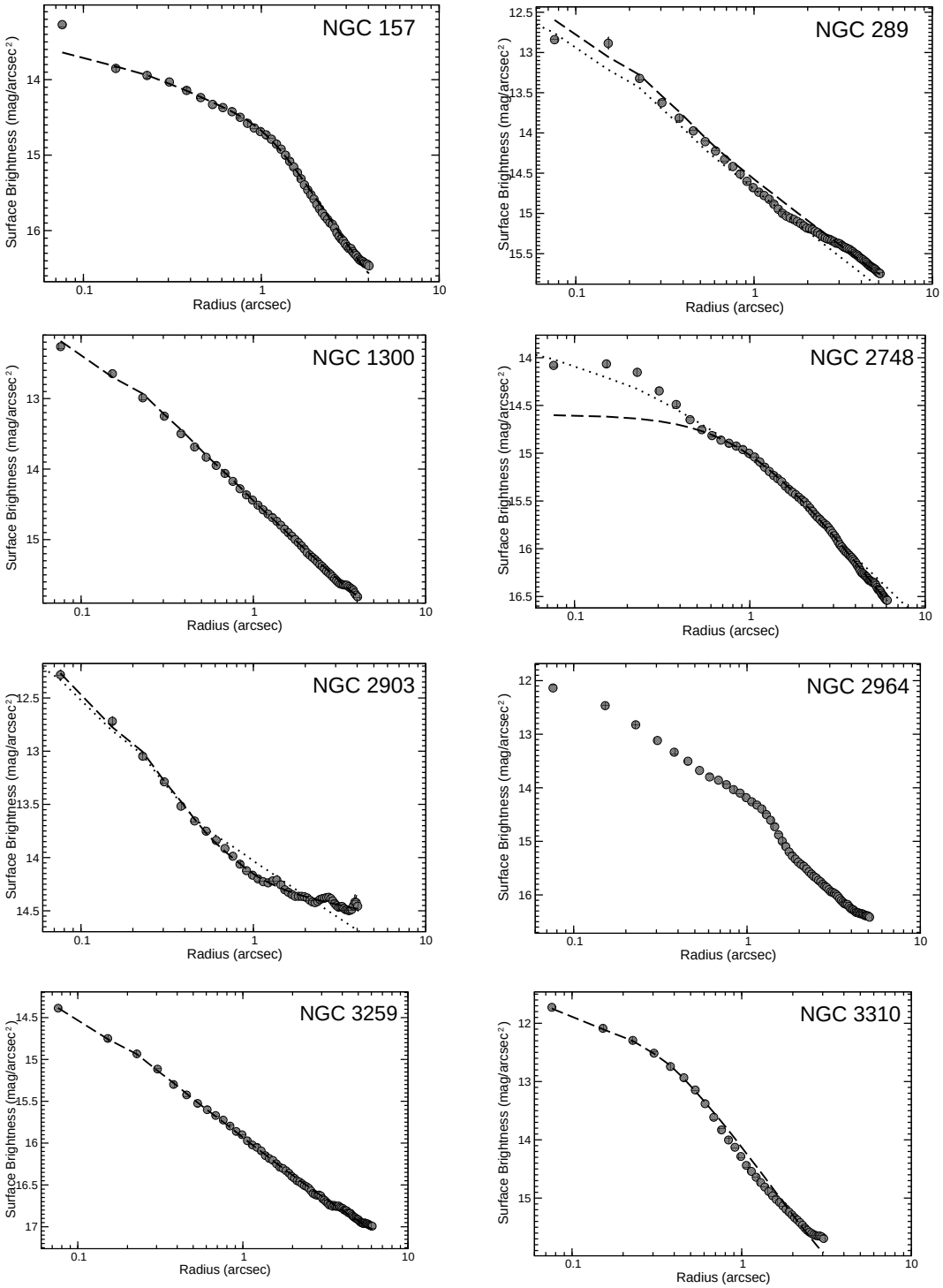

Fig. 2.— NICMOS surface brightness profiles for NGC 157, NGC 289, NGC 1300, NGC 2748, NGC 2903, NGC 2964, NGC 3259 and NGC 3310. Filled circles are the surface brightness profiles found from fitting ellipses to the isophotes. Dashed lines are our Nuker law fits to the profile and the dotted lines (NGC 289, NGC 2748 and NGC 2903) are the Nuker profile fits of Seigar et al. (2002),which which have been convolved with our Tiny Tim (Krist, Golimowski, Schroeder, & Henry 1998) generated PSFs.

2.1. Nuker Surface Brightness Profile Fits

We used the ELLIPSE program under IRAF[2] to perform isophotal ellipse fitting on the NICMOS images, from which we produced surface brightness profiles. In each case we allowed position angle and ellipticity to vary but kept the position of the center fixed.

The flux calibration of the NICMOS images was performed using conversion factors (from ADU s^{-1} to Jy) based on measurements of the standard star P330-E, taken during the Servicing Mission Observatory Verification program (M. J. Rieke 1999, private communication). Consequently, results from the ellipse fitting were converted to magnitude per arcsec^2 by:

$$m_H = -2.5 \log \left(\frac{2.19 \times 10^{-6}}{1083} \; counts \; s^{-1} \right) + 5 \log(scale) \tag{1}$$

Where *scale* is the plate scale and is 0.076 $''$pixel^{-1}. For our J-band calculations (see table 4) we substituted the factor $-2.5 \log \left(\frac{2.031 \times 10^{-6}}{1775} \; counts \; s^{-1} \right)$ into the first part of equation 1. The uncertainty on the photometry is assumed to be 2%.

To minimise assumptions, we chose to *not* mask out complicated structures such as star formation rings. Surface brightness profiles from the NICMOS images of NGC 289, NGC 2748, NGC 2903, NGC 3259, NGC 3949, NGC 4527, NGC 4536 and NGC 6384 have previously been produced, from the same raw NICMOS images, by Seigar et al. (2002). Since these galaxies are also in our sample, we re-do the profile fitting here. This enables us to perform a check on the consistency between both results. Following Seigar et al. (2002) the SBPs were fitted with a Nuker law profile, of the form introduced by Lauer et al. (1995):

$$I(r) = 2^{(\beta-\gamma)/\alpha} I_b \left(\frac{r_b}{r} \right)^{\gamma} \left[1 + \left(\frac{r}{r_b} \right)^{\alpha} \right]^{(\gamma-\beta)/\alpha} \tag{2}$$

where, β indicates the steepness of the outer profile, γ measures the steepness of the inner profile, α indicates the sharpness of the transition between these two profiles, while r_b is the point of this transition at which the SBP has a brightness of I_b.

It is important to take proper account of the NICMOS point spread function when fitting the surface brightness profiles. This can be done by either deconvolving the images prior to the fit or by convolving each model profile with a suitable psf before the fit is made. Unfortunately, deconvolution tends to increase the resultant noise. For this reason, we chose to follow the latter method, which has also been favored by other authors recently (e.g. Seigar et al. 2002; Scarlata et al. 2004). Consequently, the models were convolved with TINY TIM generated NICMOS point

[2]IRAF is distributed by the National Optical Astronomy Observatories, which are operated by the Association of Universities for Research in Astronomy, Inc., under cooperative agreement with the National Science Foundation.

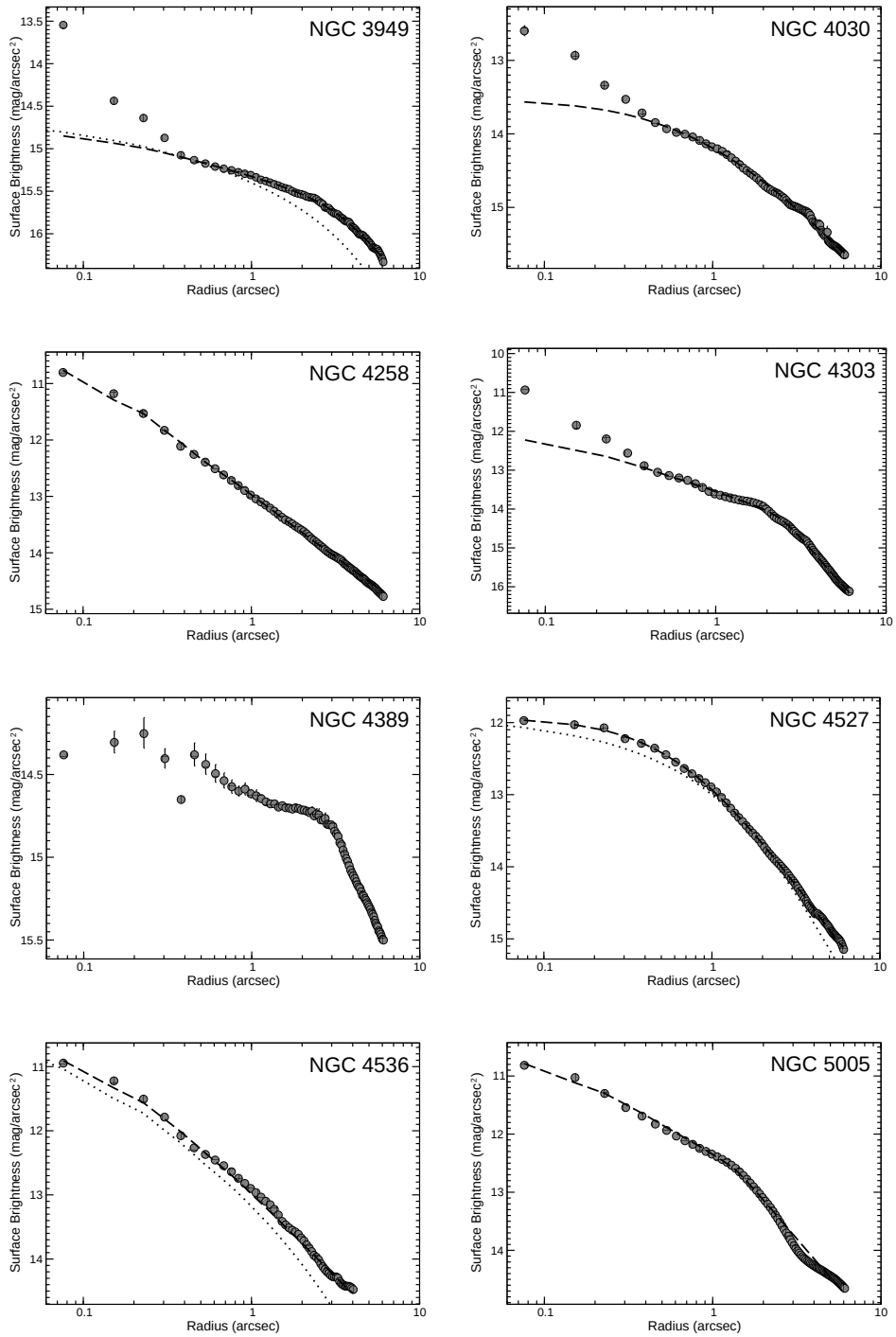

Fig. 3.— NICMOS surface brightness profiles for NGC 3949, NGC 4030, NGC 4258, NGC 4303, NGC 4389, NGC 4527, NGC 4536 and NGC 5005. The profiles have been fit with a Nuker law. Dashed lines are our fits and dotted lines (NGC 4527 and NGC 4536) are those of Seigar et al. (2002), which which have been convolved with our Tiny Tim (Krist, Golimowski, Schroeder, & Henry 1998) generated PSFs. Variations between the dotted lines and the surface brightness profiles are probably due to differing assumptions made during the isophotal ellipse fitting of the NICMOS images.

spread functions (Krist, Golimowski, Schroeder, & Henry 1998) before attempts were made to fit the surface brightness profiles.

The fitting routine is fundamentally the same as the one we used in Scarlata et al. (2004). Briefly, we constructed an IDL program that made use of the standard IDL procedure *curvefit*, which minimses χ^2 by using the Levenberg-Marquardt method to search for the best fit. The user is able to supply the inner radius at which the fit is started as well as the PSFs that are convolved with the models before each fit is attempted. As in S04, rather than add an additional model to account for central sources, we varied the inner radial range until we arrived at a suitable fit that excluded the central region and only fit the bulge. In some cases (NGC 157 and NGC 5879) we could not clearly identify a *resolved* central source, but still found that the fits were improved by varying the inner radius. Possible resolved central sources are treated separately in section 2.2.

The best profile fits are shown in Figs. 2, 3 and 4. Where possible both the Seigar et al. (2002) fits (dotted line –converted to Johnson magnitudes) and our fits (dashed line) are shown together. Following Seigar et al. (2002) we corrected for extinction using the data of Burstein & Heiles (1984).

Table 2 lists the parameters of the fits. For NGC 2964 and NGC 4389 we did not find a good fit to the surface brightness profile. In many cases, however, the SBP can be completely described by the Nuker law. Parameters from Nuker law fits performed by Seigar et al. (2002) are also included in the table. Usually we found the value of α to be poorly constrained. This is unsurprising since, in general, the range of points in the profile fits extend well beyond the break radius, r_b. This is important because as $r >> r_b$, the factor, $\left[1 + \left(\frac{r}{r_b}\right)^{\alpha}\right]^{(\gamma-\beta)/\alpha}$ tends to become independent of α.

The main reason for the differences in this work and that of Seigar et al. (2002) is the shape of the surface brightness profiles. While in part this is due to the decision as to whether or not the profiles should be smoothed, and which regions to mask, it may also be due to the subjective choices (e.g. fixing ellipticity) that have to be made when performing the isophote fits. An example of the necessary subjectivity in surface brightness profile fitting can be seen for NGC 2748. We originally interpreted the profile as showing evidence for a nuclear cluster and so start the fit at an inner radius of $0.68''$. In contrast, Seigar et al. (2002) start the profile fit inward of this and so it is unsurprising that the Nuker parameters should be different. Generally, a decision has to be made for each profile as to the region where the Nuker profile is valid. This should be inbetween any central source and the region where the galactic disk dominates. We are assuming that the Nuker profile, which Lauer et al. (1995) originally proposed to describe elliptical galaxies is actually a good description of the bulges in spiral galaxies. In some cases it is an over-complicated description of the bulge profile, while in other cases structure in the profile can produce a wide range of parameters, depending on the subjective choice as to the region over which the fitting is performed. It is also important to note that dust could give the misleading impression that a cluster is present. For example if we observe a SBP such as shown in figure 1 we must be careful that the inflexion between the apparent bulge and central source profile is not in reality a result of dust obscuration.

It is useful to compare which central sources we detect, or fail to detect, with the results we

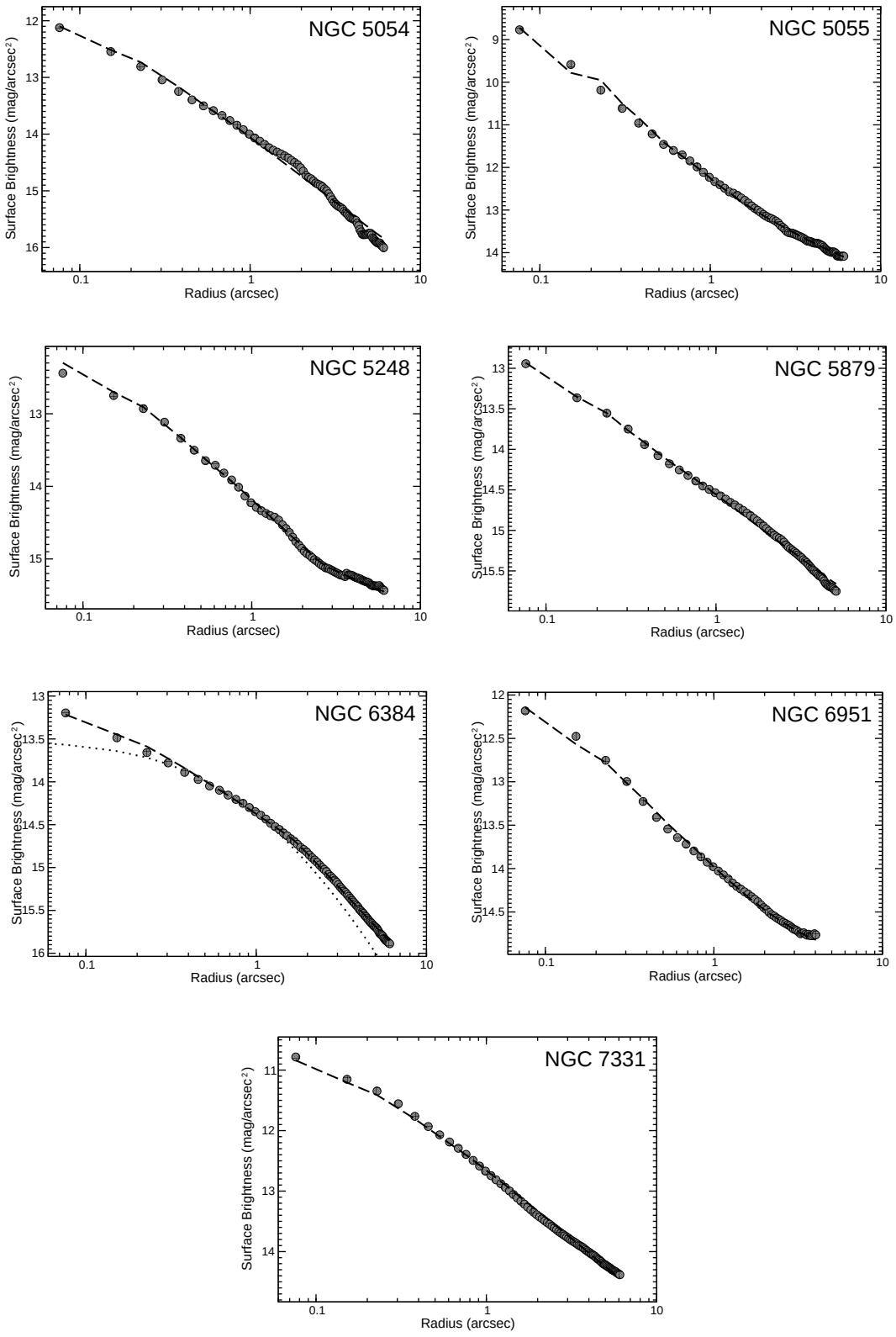

Fig. 4.— NICMOS surface brightness profiles for NGC 5054, NGC 5055, NGC 5248, NGC 5879, NGC 6384, NGC 6951 and NGC 7331. Dashed lines are our fits and dotted lines (NGC6384) are those of Seigar et al. (2002), which have been convolved with our Tiny Tim (Krist, Golimowski, Schroeder, & Henry 1998) generated PSFs. The kink in the profile of NGC 5055 at small radii is due to the convolution of the NICMOS psf with a bright point source.

presented in S04. For 4 of the galaxies; NGC 4536, NGC 5054, NGC 6384 and NGC 6951, we found central sources in the STIS profiles (shown in table 3 of S04), yet adequate Nuker law fits are made in figures 3 and 4 without the need to invoke the presence of a star cluster. There are several possibilities to explain why this situation might arise: 1) The population could be blue and hence not readily visible in the NICMOS images. 2) The presence of dust in the STIS images may have given us the misleading impression of a cluster being present 3) An older, redder population may dominate the NICMOS images to an extent that the cluster is not visible 4) The lower resolution of the NICMOS images may have smoothed out any image of the cluster.

The presence of central sources seems clear for NGC 2748, NGC 3949, NGC 4030 and NGC 4303, where a well sampled[3] upturn in the profile in the NICMOS images is present. However, closer inspection of the NICMOS images in figure 5 shows that dust is the likely cause of the inflexion in the SBP for NGC 2748. This highlights the problem of using just the surface brightness profile to find central sources. Central sources for all of the remaining galaxies were previously reported in S04, though only the cluster in NGC 4030 was identified as resolved in that paper[4]. A central star cluster has also been identified by Colina et al. (2002) for NGC 4303, who find a 3.1 pc cluster of 4 Myrs in age. In figure 6 the SBPs are compared with the NICMOS point spread function, and appear to be resolved. In these cases, if the Nuker law describes the underlying galactic light, the magnitude of the central source can be extracted.

2.2. Quantifying the Size and Luminosity of the Central Sources

We attempted to quantify the size and luminosity of the central sources. Specifically, the techniques we used are similar to those described in S04, which were derived from the analysis of Carollo, Stiavelli, & Mack (1998). The results are shown in Table 3. In summary, the luminosity of the central source is bounded by the results from two methods. In the first method a Gaussian profile is fit to each central source using the IRAF task N2GAUSSFIT[5]. This task also calculates the background and so we produced background-subtracted model Gaussian central sources, from which the luminosity could be determined. In the second method, the profile fits from Table 2 were used to produce model images of the galaxy bulges. These were then subtracted from the original galaxy images and the luminosity of the central source was determined by using an aperture size

[3]The surface brightness profile for NGC 157 also shows an excess above the Nuker fit, but in this analysis the excess is defined by a single point only. Since our goal is to find resolved sources we did not investigate it further.

[4]Note that in S04 point sources were defined to be those that have FWHM $\leq$ (1.5 $\times$ FWHM$_{PS}$), where FWHM$_{PS}$ means for a point source. Here we consider all sources with FWHM larger than the PSF to be at least, marginally resolved. Consequently, if we applied the S04 definition NGC3949 and NGC4303 would also be classified as point sources in Table 3

[5]The sides of the box, over which the Gaussians were fit to the images, were set to $\sim 8\times$ FWHM of the NICMOS PSF.

Table 2. Parameters from NUKER law fits.

NGC	range ($''$)		α		β		γ		R_b ($''$)		I_b (mag/$''^2$)	
0157	0.15-6.08	—	6.83	—	1.38	—	0.45	—	1.05	—	14.69	—
0289	0.08-6.08	(0.0-5.0)	47.67	(12.22)	0.67	(0.69)	0.92	(0.91)	0.72	(0.60)	14.34	(15.68)
1300	0.08-6.08	—	73.20	—	0.89	—	0.99	—	0.95	—	14.42	—
2748	0.68-6.08	(0.0-8.0)	1.75	(5.01)	0.97	(0.71)	0.00	(0.46)	0.89	(0.86)	14.94	(16.31)
2903	0.08-4.03	(0.0-5.0)	2.92	(20.22)	0.13	(0.43)	0.99	(0.95)	0.74	(0.43)	14.02	(14.99)
3259	0.08-6.08	(0.3-8.0)	0.23	(7.33)	0.14	(0.68)	1.29	(0.44)	0.23	(0.00)	14.86	(15.60)
3310	0.08-2.51	—	88.74	—	1.51	—	0.74	—	0.38	—	12.60	—
3949	0.46-6.08	(0.3-8.0)	3.07	(1.53)	1.10	(2.57)	0.23	(0.26)	3.74	(7.44)	15.86	(18.39)
4030	0.61-6.08	—	0.88	—	1.12	—	0.00	—	1.12	—	14.25	—
4258	0.08-6.08	—	32.94	—	0.87	—	1.01	—	0.48	—	12.28	—
4303	0.53-6.08	—	10.13	—	2.00	—	0.62	—	2.38	—	14.23	—
4527	0.08-6.08	(0.0-8.0)	1.33	(1.61)	1.33	(1.79)	0.01	(0.27)	0.58	(1.51)	12.46	(14.76)
4536	0.08-4.03	(0.0-8.0)	0.39	(2.13)	1.26	(2.06)	0.67	(0.91)	0.59	(2.43)	12.44	(15.76)
5005	0.08-3.04	—	130.83	—	1.34	—	0.71	—	1.37	—	12.59	—
5054	0.08-6.08	—	0.04	—	1.62	—	0.14	—	0.39	—	13.17	—
5055	0.08-6.08	—	1.02	—	0.58	—	1.62	—	1.08	—	12.41	—
5248	0.08-3.04	—	98.30	—	0.41	—	0.85	—	2.66	—	15.09	—
5879	0.15-5.09	—	8.16	—	0.63	—	0.87	—	0.27	—	13.63	—
6384	0.08-6.08	(0.3-8.0)	452.89	(0.76)	0.85	(1.78)	0.54	(0.01)	1.7	(2.00)	14.74	(16.32)
6951	0.08-4.03	—	1.33	—	0.00	—	0.88	—	3.11	—	14.79	—
7331	0.08-6.08	—	0.11	—	1.62	—	0.19	—	1.94	—	13.22	—

Note. — The Nuker law parameters as defined in Eq. 2. Range is the region, in arcseconds, over which the fits were made. I_b has been corrected using Burstein & Heiles (1984) results. The values in parenthesis are taken from Seigar et al. (2002) and are presented here for comparison. Note: the quoted I_b values from Seigar et al. (2002) remain in the AB magnitude system, while ours are quoted in the Johnson system.

of approximately 2×FWHM of the central source.

As in S04 we used the Plummer law to determine the half-light radius, b, of the central sources.

$$I_P(r) = \frac{L}{\pi b^2}\left(1+\frac{r^2}{b^2}\right)^{-2} \tag{3}$$

Here, I is the total luminosity of the central source and r is the radius from the center of the source. We do not directly measure b, instead we determine the FWHM from Gaussian fits to the central sources. To convert our results to the half-light radius b, we repeat the method described in S04. Briefly, we established the relationship between the Gaussian FWHM and b by simulating multiple central sources of known b. These artifical images of star clusters were convolved with a NICMOS PSF and the FWHMs determined in the same way as the actual images. The uncertainties on b were found by varying the sides of the box, over which the Gaussians were fit to the original images, by ± 2 pixel

3. The Age of the Central Stellar Populations

The main goal of our STIS project is to understand the nature of the central regions of a sample of nearby late type spirals, and to determine whether the galaxies host a black hole in their centers. Using the STIS spectroscopic data we are carrying out detailed modelling of the central velocity field of the nuclear disks in our sample of galaxies to infer the central mass concentrations. Before we can conclude that the central mass is a black hole we need to determine whether such a central mass concentration could be accounted for by a stellar population.

As a first step towards finding the masses of the central stellar populations we need to quantify their ages. Due to the difficulties in identifying nuclear clusters from the NICMOS images, and since some star clusters may be present but completely hidden by the bulge light we decided to examine the central stellar population within two arbitrary, but small, apertures of diameters 50 pc and 100 pc. Galaxies for which no obvious central source was seen in the NICMOS SBP are also included. The magnitudes within these circular apertures, plus magnitudes within annuli of the same area directly surrounding the apertures are shown in Table 4.

The near infrared data are useful for investigating the masses of stellar populations for two main reasons. First, the extinction in the H-band is greatly reduced in comparison with that in the optical ($A_H = 0.175 A_V$, Rieke & Lebofsky 1985). Second, the infrared mass-to-light ratios are less dependent on the galaxy properties than the optical ones. Still they can vary by a factor of 2 (see e.g., Bell & de Jong 2001), so an estimate of the age of the stellar population is necessary.

We used Starburst99 (Leitherer et al. 1999) evolutionary synthesis models. Our goal is not to constrain the IMF, so we used just the standard Salpeter IMF with an upper mass cutoff of $M_{\rm up} = 100\,{\rm M}_\odot$. The model assumes solar metallicity and instantaneous star formation. For the

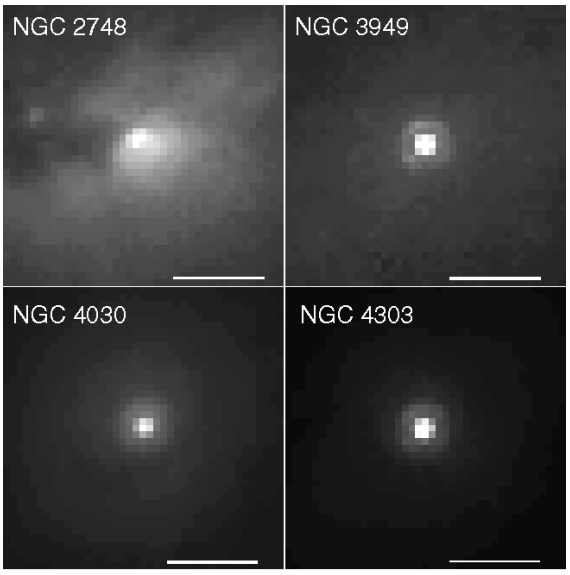

Fig. 5.— The archival NICMOS f160w images for the 4 central source candidates. Cut levels have been adjusted to highlight the nuclei. The white bar shows a scale of 1 ″. The image for NGC 2748 shows that the presence of significant amounts of dust is the likely cause of the inflexion in the surface brightness profile. The central sources in the other galaxies are not much different to the size of the NICMOS PSF (see also figure 6), as can be seen by the presence of Airy rings

Table 3. Properties of the Central Sources.

Galaxy	M_H (mag)	M_R (mag)	b (pc)	b_R (pc)	FWHM (arcsec)	FWHM (R) (arcsec)
(1)	(2)	(3)	(4)	(5)	(6)	(7)
NGC 3949	-14.1±0.2	...	$1.7^{+0.2}_{-0.4}$	PS	0.17	...
NGC 4030	-16.6±0.2	-14.0 ± 0.3	$9.8^{+0.9}_{-1.1}$	7.6 ± 0.2	0.32	0.16
NGC 4303	-18.0±0.2	...	$4.5^{+0.2}_{-0.2}$	PS	0.19	...

Note. — (1): The name of the galaxy. (2): The absolute H-band magnitude. (3): The equivalent absolute STIS R-band magnitude from S04. (4) The half-light radius from the plummer law shown in equation 3. The value in parenthesis is from the STIS R-band results of S04, converted to the H_0 used here. PS means point source. (5): The half-light radius from S04. (6): The Full Width Half-Maximum from the Gaussian fits. (7): The Full Width Half-Maximum from S04. Note that values from S04 have been converted using H_0=75 km s^{-1}

6 galaxies with two observed colors (R-H and J-H) we can plot a two color diagram and compare with the model outputs. The NICMOS magnitudes are measured in the Johnson photometric system whereas the STIS acquisition magnitudes are given in the STMAG photometric system. We have used the Starburst99 spectral energy distribution outputs to convert the STIS acquisition magnitudes to the R band using the synphot package in IRAF.

As can be seen from Table 4 there is no strong variation of the color whether the 50 pc or 100 pc aperture is used. Figure 7 shows the R-H against J-H colors for the 100 pc aperture size. The time evolution for ages between 1 Myr (lower left corner) and 20 Myr (in intervals of 1 Myr) and for 30 and 40 Myr are shown for the three models described above. For reference the reddest values for the R-H color occur for ages of between 9 and 12 Myr, which correspond to the epoch when the first supergiants appear and start contributing significantly to the light in the H-band. We also show in this diagram the effect of one magnitude of extinction. Unfortunately the results cannot distinguish between the models. The reddening vector is almost parallel to the models and so with the right amount of extinction the points could fit a variety of ages. Clearly the R-J and J-H colors alone cannot be used to constrain the age of the stellar population.

A better way to constrain the age of the stellar population is to use the equivalent width of Hα. Table 4 shows the EW within square apertures defined by sides of 50 pc (or 100 pc) and the slit width of $0.2''$. As can be seen from figure 83 in Leitherer et al. (1999), for instantaneous star formation the EW of Hα decreases with time. Figure 8 shows the R-H color against Hα equivalent width. Here we plot the data for the 14 galaxies with measured colors and EWs. Again the evolution is shown for ages between 1 and 20 Myr (in 1 Myr intervals) and 30 and 40 Myr. Note that in this case the extinction vector only affects the color because we are assuming that the extinction to the stars and the gas is the same, and thus the equivalent width of the line is independent of the extinction. The Hα equivalent width allows the ages of the stellar population to be constrained. We can also infer the extinction to the central 100 pc. The typical values for our sample are $A_V = 1 - 2$ mag. The derived ages of the central sources (they are mostly independent of the model assumed) are typically between 10 and 15 Myr, except for NGC 3310 where the age is 6-7 Myr.

The case of continuous star formation was ruled out since the Starburst99 (Leitherer et al. 1999) simulations indicate that the equivalent width of Hα should remain greater than 146 Å, which is not the case for any of the galaxies in our sample. We also believe that the case of an older stellar population plus continuous star formation is not the case in the central regions due to the similarity in colors in both 50 pc and 100 pc apertures.

Note however that the underlying assumption is that all the ionizing photons come from stars. If an active galactic nucleus were present then this would tend to increase the equivalent width and give the impression that a stellar population was actually younger than its real age. We cannot unambiguously rule out previously unknown AGN in the galaxies in our sample. As a check, using our data we examined the line ratios of both [N II] (λ6550,6585 Å) and [S II] (λ6718,6732 Å)

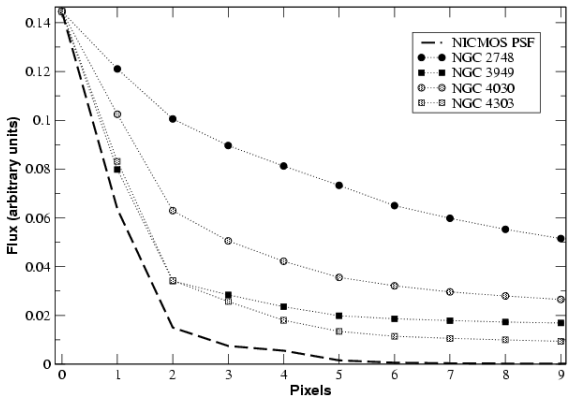

Fig. 6.— Comparison of light profiles of those galaxies that seem to harbor compact sources with the NICMOS point spread function (PSF). The NICMOS profile was generated using the TINY TIM software package (Krist, Golimowski, Schroeder, & Henry 1998). The profiles have been scaled so that the fluxes are equal at the central pixel. No attempt has been made to extract the underlying bulge light.

Table 4. Magnitudes within a circular aperture and equivalent widths of Hα

Galaxy	**R 50pc**	**R 100pc**	**R(a) 50pc**	**R(a) 100pc**	**R-H 50pc**	**R-H 100pc**	**R-H(a) 50pc**	**R-H(a) 100pc**	**J-H 50pc**	**J-H 100pc**	**EW(Å) 50pc**	**EW(Å) 100pc**
NGC 0289	18.40	17.38	18.98	17.93	3.61	3.61	3.64	3.36	1.14	1.17	20.1 (0.5)	18.6 (0.3)
NGC 1300	17.47	16.51	18.07	17.25	3.15	3.15	3.15	3.11	...	...	5.1 (0.1)	4.0 (0.1)
NGC 2748	...	...	...	...	...	...	...	...	...	...	55 (2)	35.7 (0.9)
NGC 2903	16.80	15.68	17.32	15.90	3.55	3.55	3.45	3.31	...	...	9.3 (0.1)	12.6 (0.2)
NGC 2964	17.61	16.57	18.14	17.16	3.31	3.31	3.24	3.18	...	...	10.6 (0.1)	16.7 (0.3)
NGC 3259	19.65	18.62	20.15	19.12	2.72	2.72	2.88	2.83	...	...	53.8 (0.7)	37 (1)
NGC 3310	16.42	15.47	16.92	16.59	2.92	2.92	2.86	2.84	0.93	0.92	75 (1)	75 (1)
NGC 3949	18.08	17.04	18.68	17.41	2.64	2.64	2.61	2.66	0.87	0.89	...	...
NGC 4030	17.83	16.85	18.47	17.29	3.10	3.10	3.19	3.15	...	...	2.43 (0.06)	2.66 (0.04)
NGC 4258	15.08	14.18	15.79	14.92	3.14	3.14	3.02	2.93	0.97	0.96	29.1 (0.4)	24.1 (0.4)
NGC 4303	16.22	15.59	17.47	16.61	2.71	2.71	3.11	3.03	...	...	5.7 (0.9)	6.9 (0.1)
NGC 4536	17.52	16.51	18.01	17.22	4.18	4.18	4.12	4.03	...	...	1.29 (0.02)	1.86 (0.03)
NGC 5005	16.07	14.88	16.34	15.40	3.63	3.63	3.34	3.37	...	...	12.1 (0.2)	8.7 (0.4)
NGC 5054	17.93	16.92	18.52	17.50	3.47	3.47	3.51	3.35	...	...	3.07 (0.08)	3.35 (0.08)
NGC 5055	14.44	13.85	15.63	15.17	3.78	3.78	3.69	3.83	...	...	...	...
NGC 5248	17.25	16.29	17.84	17.03	3.08	3.08	3.19	3.20	...	...	4.40 (0.08)	3.8 (0.1)
NGC 5879	17.76	16.62	18.18	16.94	3.25	3.25	3.13	2.95	...	...	3.0 (0.1)	2.26 (0.03)
NGC 6384	18.71	17.46	19.02	17.75	3.23	3.23	3.13	3.11	0.97	0.99	...	...
NGC 6951	17.64	16.71	18.30	17.35	3.54	3.54	3.64	3.60	1.07	1.12	12 (1)	13 (1)
NGC 7331	15.07	14.19	15.83	14.97	3.17	3.26	3.26	3.20	...	...	1.32 (0.08)	1.01 (0.02)

Note. — Magnitudes calculated within circular apertures. The diameter of the apertures is given in parenthesis. R(a) indicates that the magnitudes are found for annuli of area equivalent to a circular aperture of the given diameter. e.g. 'R(a) 50 pc' is the magnitude within an annulus that begins at 25 pc from the nucleus and has an area equivalent to a 50 pc circular aperture. The right-most columns denote the equivalent widths of Hα for the sum of the signal within square apertures with sides of 50 pc and 100 pc respectively.

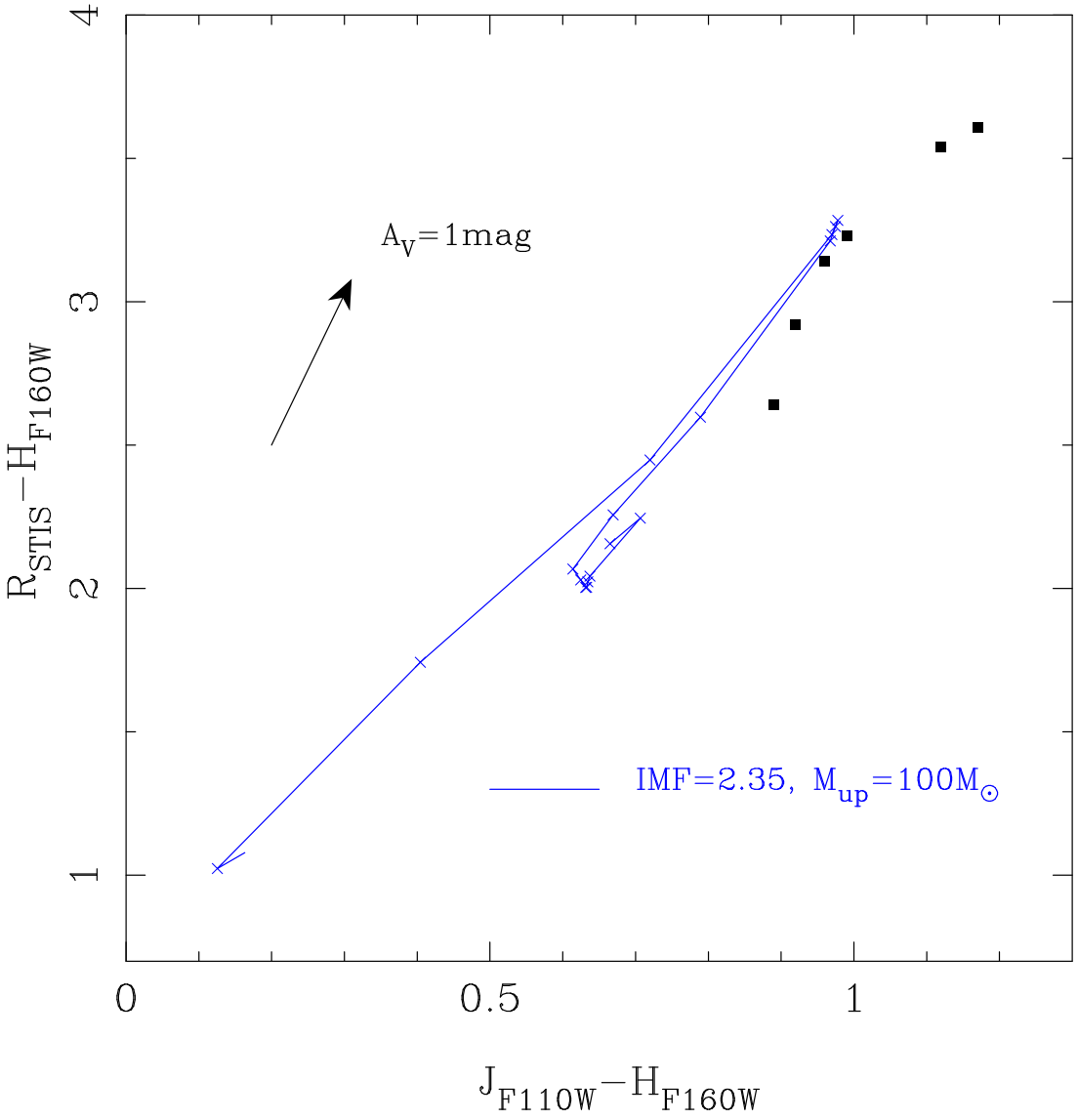

Fig. 7.— The color indices were compared to the models of Leitherer et al. (1999). The plot shows the stellar evolutionary models for an instantaneous burst of star formation, for a Salpeter initial mass function with lower and upper mass cutoffs of 1 and 100 $M_\odot$, respectively.

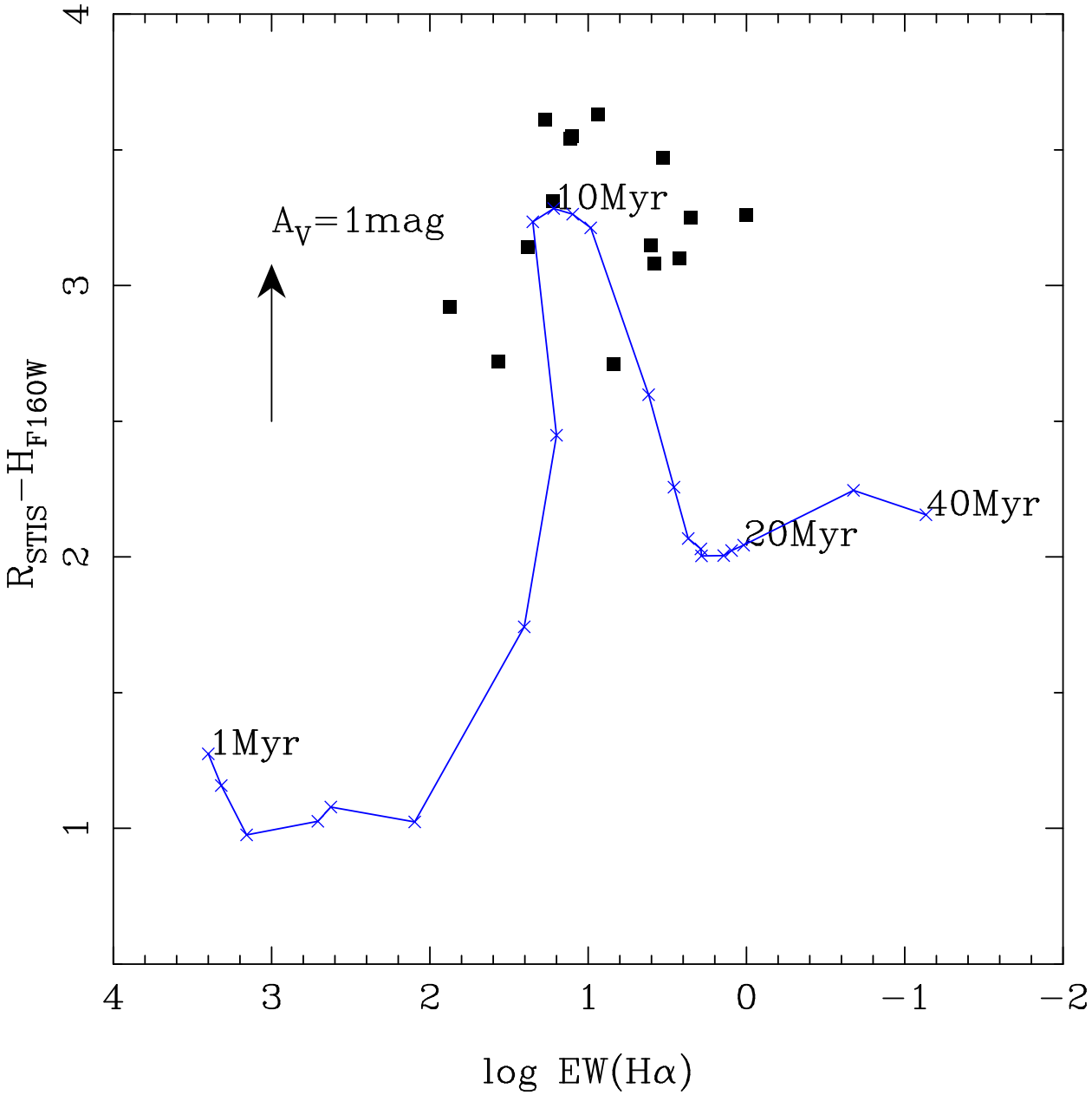

Fig. 8.— The R-H color index against Hα equivalent width for 100 pc apertures placed on the on-nucleus spectra. The model population is the same as in figure 7. This is much more useful than the plot in figure 7 as it suggests the age range of the central stellar populations is ∼10-20 Myr. The points correspond to those galaxies where both color and $H\alpha$ spectral information was available and not just those with obvious central sources apparent in their surface brightness profiles.

Table 5. Line Flux ratios relative to Hα

Galaxy Name	Activity Status	[N II] (6549.85 Å)	[N II] (6585.28 Å)	[S II] (6718.29 Å)	[S II] (6731.67 Å)
NGC1300	... (...)	0.83 (0.03)	1.83 (0.03)	0.82 (0.02)	0.65 (0.02)
NGC2748	... (H II)	0.182 (0.003)	0.370 (0.005)	...	...
NGC2903	H II (H II)	0.16 (0.01)	0.507 (0.004)	...	...
NGC2964	H II (H II)	0.211 (0.002)	0.556 (0.002)	0.184 (0.003)	0.174 (0.003)
NGC3310	H II (H II)	0.192 (0.002)	0.587 (0.002)	0.121 (0.001)	0.125 (0.002)
NGC4258	H II (H II)	0.49 (0.02)	0.77 (0.01)	0.214 (0.003)	0.24 (0.003)
NGC4303	H II/S2 (H II)	1.886 (0.006)	1.044 (0.004)	0.487 (0.002)	0.456 (0.004)
NGC4536	H II (H II)	...	1.81 (0.02)	0.53 (0.01)	1.06 (0.02)
NGC5005	S2/L (L1.9)	2.17 (0.07)	5.0 (0.2)	1.10 (0.04)	1.57 (0.05)
NGC6951	L/S2 (S2)	1.36 (0.02)	4.30 (0.05)	0.69 (0.01)	0.79 (0.01)

Note. — ine Flux ratios, calculated by dividing the corresponding Hα (6564.61Å) flux. All wavelengths are for a vacuum. Uncertainties were calculated by repeating each flux measurement a minimum of 10 times and are shown in parenthesis. The current activity status values are repeated from Table 1 and are taken from the NASA Extragalactic Database (NED) with classification shown in parenthesis taken from Ho, Filippenko, & Sargent (1997), where H II=H II nuclei, S=Seyfert nuclei and L=LINER.

to that of H α (λ6565 Å). The results are presented in Table 5. Two possible additional weak AGN, indicated by the relatively high values of the [N II] ratios are NGC 1300 and NGC 4536. It should also be noted that the galaxies with known activity in our sample have EWs that are well spread throughout the distribution of equivalent widths (e.g. EW=24.1±0.4 for NGC 4258 and EW=1.01±0.02 for NGC 7331). In summary, while we think it is unlikely that the equivalent widths are dominated by ionization from weak nuclear activity we cannot rule it out with this dataset.

4. Summary

Using NICMOS images we constructed surface brightness profiles, to which we fitted Nuker laws to search for the presence of nuclear star clusters. Several of the images had previously been fit by Seigar et al. (2002) and there is some variation in their resultant Nuker parameters when compared with ours partly due to the necessary subjectivity in performing the fits. In 4 cases; NGC 2748, NGC 3949, NGC 4030 and NGC 4303 there appears to be an excess which can not be accounted for by the Nuker profile alone. In the case of NGC 2748 the apparent excess is misleading and is probably due to obscuring dust causing an inflexion in the surface brightness profile. However, for the latter 3 galaxies the excesses are likely to be real and may be due to the presence of nuclear star clusters.

Although star clusters and AGN can coexist (e.g. Colina et al. 2002) we attempted to identify any unknown AGN by using [N II] and [S II] line flux ratios (relative to Hα) and found tentative evidence for weak AGN in NGC 1300 and NGC 4536.

As a first step towards constraining the ages of the central stellar populations we used color information from the STIS and NICMOS images and the equivalent width of Hα for the STIS spectra and compared these data to the stellar evolutionary models of Leitherer et al. (1999). The equivalent width of Hα was the important factor as it constrained the ages to $\sim$10 Myr provided that the ionization of the disk was primarily due to the central stellar population. To confirm the age of the population we would need to perform spectroscopy on the galaxy centers.

5. Acknowledgments

MAH thanks A Robinson and R. van der Marel for their comments and suggestions. MAH particularly thanks Jim Collett for very useful discussions. We would also like to thank the anonymous referee for valuable suggestions which improved this paper. We have made use of the LEDA database (http://leda.univ-lyon1.fr). This research has made use of the NASA/IPAC Extragalactic Database (NED) which is operated by the Jet Propulsion Laboratory, California Institute of Technology, under contract with the National Aeronautics and Space Administration.

REFERENCES

Atkinson, J. et al. 2004, MNRAS, in press.

Bell, E. F. & de Jong, R. S. 2001, ApJ, 550, 212

Böker, T., van der Marel, R. P., Mazzuca, L., Rix, H., Rudnick, G., Ho, L. C., & Shields, J. C. 2001, AJ, 121, 1473

Böker, T., Laine, S., van der Marel, R. P., Sarzi, M., Rix, H., Ho, L. C., & Shields, J. C. 2002, AJ, 123, 1389

Burstein, D. & Heiles, C. 1984, ApJS, 54, 33

Carollo, C. M. & Stiavelli, M. 1998, AJ, 115, 2306

Carollo, C. M., Stiavelli, M., & Mack, J. 1998, AJ, 116, 68

Carollo, C. M., Stiavelli, M., Seigar, M., de Zeeuw, P. T., & Dejonghe, H. 2002, AJ, 123, 159

Colina, L., Gonzalez Delgado, R., Mas-Hesse, J. M., & Leitherer, C. 2002, ApJ, 579, 545

Ferrarese, L. & Merritt, D. 2000, ApJ, 539, L9

Gebhardt, K., et al. 2000, ApJ, 539, L13

Ho, L. C., Filippenko, A. V., & Sargent, W. L. W. 1997, ApJS, 112, 315

Hughes, M. A. et al. 2003, AJ, 126, 742

Kormendy J., Richstone D., 1995, ARA&A, 33, 581

Krist, J. E., Golimowski, D. A., Schroeder, D. J., & Henry, T. J. 1998, PASP, 110, 1046

Lauer, T. R. et al. 1995, AJ, 110, 2622

Leitherer, C. et al. 1999, ApJS, 123, 3

Marconi, A. et al. 2003, ApJ, 586, 868

Marconi, A. & Hunt, L. K. 2003, ApJ, 589, L21

McLeod, B. A. 1997, The 1997 HST Calibration Workshop with a new generation of instruments /edited by Stefano Casertano, Robert Jedrzejewski, Charles D. Keyes, and Mark Stevens. Baltimore, MD : Space Telescope Science Institute (1997) QB 500.268 C35 1997, p. 281., 281

Phillips, A. C., Illingworth, G. D., MacKenty, J. W., & Franx, M. 1996, AJ, 111, 1566

Rieke, G. H. & Lebofsky, M. J. 1985, ApJ, 288, 618

Scarlata, C., et al. 2004, AJ, 128, 1124

Seigar, M., Carollo, C. M., Stiavelli, M., de Zeeuw, P. T., & Dejonghe, H. 2002, AJ, 123, 184

Walcher C. J., Häring N., Böker T., Rix H.-W., van der Marel R., Gerssen J., Ho L. C.,Shields J. C., 2003, Carnegie Observatories Astrophysics Series, Vol. 1: Coevolution of Black Holes and Galaxies, ed. L. C. Ho (Pasadena: Carnegie Observatories, http://www.ociw.edu/ociw/symposia/series/symposium1/proceedings.html)